Earth, Planets and Space

FULL PAPER Open Access

Analysis of a secondary 16-day planetary wave generation through nonlinear interactions in the atmosphere

Kseniia A. Didenko[1,2*], Andrey V. Koval[2,3], Tatiana S. Ermakova[2,3], Arsenii V. Sokolov[2] and Olga N. Toptunova[2,3]

Abstract

Using a nonlinear model of the general circulation of the middle and upper atmosphere (MUAM), spatio-temporal structures of planetary waves (PWs) during boreal winter were studied. Modeling of global atmospheric circulation was performed for January–February. Despite the tropospheric PW sources shaped in the model, the phenomenon of 16-day PW excitation arise out of internal atmospheric sources in the southern lower thermosphere was discovered. To explain the observed phenomenon, a number of numerical experiments were carried out according to different scenarios with a selective turning (on/off) tropospheric sources of PW individual modes (having periods of 4–16 days) in the model. Also, the evolution of perturbed potential enstrophy for a 16-day PW, as well as the contribution of nonlinear interactions between individual PW to it, was studied. This made it possible for the first time to demonstrate explicitly the process of generation a secondary 16-day PW as a result of the nonlinear interconnection of 4-day and 5-day PWs.

Keywords Planetary waves, Atmospheric normal modes, Nonlinear interaction, Numerical simulation, Potential enstrophy

*Correspondence:
Kseniia A. Didenko
didenko@izmiran.ru
Full list of author information is available at the end of the article

Graphical Abstract

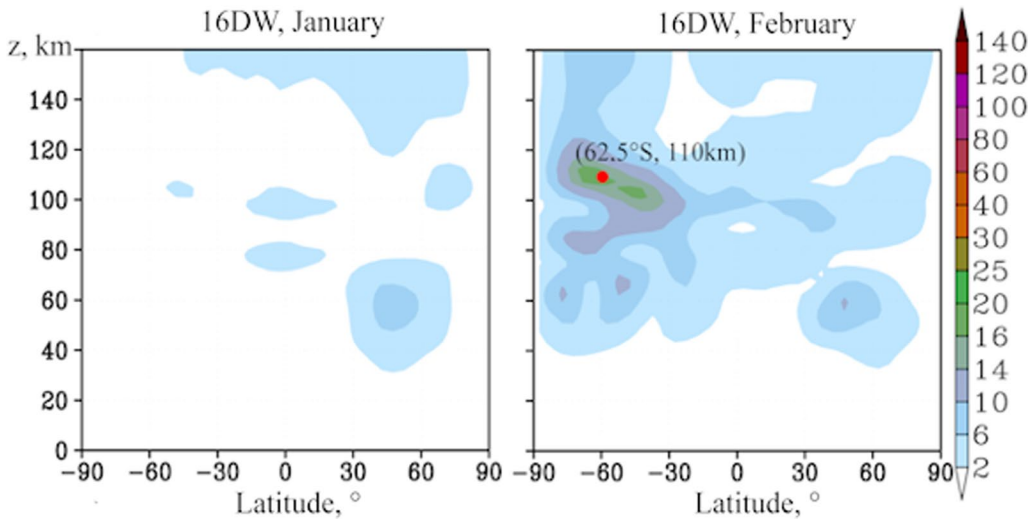

1 Introduction

Planetary waves (PWs) cause the longitudinal variations of atmospheric parameters. PWs represent periodic changes in all hydrodynamic quantities, i.e., wind, temperature, pressure, density, and are classified on the bases of the temporal and spatial scales. PWs are formed due to the latitudinal gradient of potential vorticity and are characterized by different zonal wave numbers (an integer of waves that fall on the circle of latitude). Transferring energy and momentum, while propagating upwards from their sources, PWs significantly affect the general atmospheric circulation, temperature mode and composition throughout the entire layer of the middle and upper atmosphere reaching by its influence the mesosphere and lower thermosphere heights, and are also a foundational aspect of atmospheric meridional circulation in extratropical region (Haynes et al. 1991; Holton et al. 1995). The propagation of PWs during boreal winter due to the increase in wave activity contributes to the formation of specific types of atmospheric phenomena such as sudden stratospheric warming (SSW) (Nath et al. 2016; Baldwin et al. 2021) when interacting with the general circulation. PWs are also an important link in transmitting a signal from a quasi-biennial oscillation of the equatorial zonal wind (QBO) (Koval et al. 2022) and/or from El Nino Southern Oscillation (ENSO) (e.g., Ermakova et al. 2019) up to the polar latitudes.

Another important outcome of the planetary waves' upward propagation, accompanied by an increase in their amplitudes complimented by an atmospheric density decrement, is the occurrence of various nonlinear processes. Generation of secondary planetary waves, through nonlinear interconnections of waves and waves with the mean flux is an example of such processes. Numerous studies of PWs (see, for example, Jacobi et al. 1998; Pancheva 2000; Forbes and Zhang 2017; Forbes et al. 2020; He et al. 2020) including atmospheric tides showed the existence of secondary waves, which are the sum or difference of waves rallied into nonlinear interconnections. It was shown that the mechanism of atmospheric tides modulation as an effect of nonlinear interconnections of the atmospheric solar tide and the PW is a quadratic nonlinear process (Teitelbaum and Vial 1991). This theory was applied to the study of interactions between such waves having a large or global scale as atmospheric normal (resonant) modes (NMs) and Rossby waves in Pogoreltsev (2001); He and Forbes (2022).

The idea of wave interactions as a quadratic nonlinear process was proposed by Smith (1983) and further developed by Pogoreltsev (2001) and Didenko et al. (2022) to describe the variability of the squared potential vorticity (or enstrophy) in stratosphere of the Northern Hemisphere during its winter. Planetary waves' amplification in the troposphere, the lower stratosphere, accompanied by variations in wind fields through which PW propagates, leads to the SSW onset. Potential vorticity transfer process between waves occurs to provide the energy balance or the potential enstrophy balance under the evolution of such extreme events. The previous studies have demonstrated the need to analyze nonlinear wave interactions along with the interactions of waves with the

mean flux through the SSW studies (Labitzke and Kunze 2009; Pogoreltsev et al. 2015).

In recent work by Koval et al. (2023), a description of simulation experiments during the initialization of the model for boreal winter conditions (January–February) is presented and the formation of atmospheric global circulation, taking into account the comparative contribution of different modes of planetary waves is defined. The results allowed quantifying how various hydrodynamic fields, in particular, zonal wind and temperature, respond to the inclusion of various PW sources in the model of the general circulation MUAM. The mode choice under the boreal winter conditions was imposed by the well-known fact that PWs wave activity increase during this period: PW waveguides are localized in the atmosphere areas where the difference between the wave phase velocity and the wind speed is positive, according to the formula for refractivity index (e.g., Albers et al. 2013). That is why winter background conditions with westerly winds in the stratosphere are favorable for the PW propagation. However, it was in the Southern (summer) Hemisphere that the effect was found when analyzing model runs, showing the unexpected generation process of the 16-day wave as a result of the internal atmospheric sources influence, although tropospheric sources of this wave were not specified in this run. The purpose of this work is to study the reasons for this wave arising, as well as to evaluate the efficiency of the quadratic nonlinear process of secondary PWs generation in the middle and upper atmosphere. The transfer of eddy potential enstrophy between wave modes during the development of nonlinear wave processes was taken into consideration to explain the observed effects.

2 Methods and approaches

2.1 The MUAM model

A number of numerical experiments were carried out with the Middle and Upper Atmosphere Model (MUAM, Fröhlich et al. 2003; Pogoreltsev et al. 2007; Koval et al. 2022) to study the global and the regional circulation of the atmosphere and the planetary waves' impact thereon. MUAM as a nonlinear three-dimensional mechanistic model allows simulating the general circulation in the atmospheric region from the surface to the levels of 300–400 km, that is, to the ionospheric heights of the F2 layer. Currently, the model keeps developing, a parameterization of atmospheric heating rates due to the release of latent heat, which takes into consideration as daily and longitude variations and the El Nino–Southern Oscillation (ENSO) phase relation has been included (Ermakova et al. 2017). Special attention in the model is given to atmospheric wave dynamics. This enables the middle and upper atmosphere processes of interconnections of waves with the mean flux, as well as the role of PW in the propagation of various external influences (QBO, ENSO, variations in solar activity, etc.) on global spatial scales to be complete investigated (Gavrilov et al. 2018; Medvedeva et al. 2019; Koval et al. 2018a; 2022; 2023). The ability both to analyze the amplitudes of planetary waves and to link these waves with different sources of origin is one of the MUAM advantages. Four-dimensional fields (time step is 2 h) of geopotential, three components of wind speed vector and temperature are the main parameters calculated by the model.

Horizontal resolution in latitude and longitude of MUAM as finite-difference model is 5°×5.625°, respectively. Using pressure scale height—H, the surface pressure—ps, pressure in hPa—p, a dimensionless log-isobaric vertical coordinate or height can be obtained by the formula $x = -Hln(p/ps)$. While the upper boundary varies from 135 to 300–400 km depending on solar activity and thermospheric temperature, the quantity of vertical levels is also ranging (48–60 levels). The Marchuk-Strang technique of splitting (Strang 1968) is used to solve prognostic equations, and the Matsuno scheme (Matsuno 1966) is used for the integration in time with a time-step of 225 s. The model with 56 vertical levels version spanning an atmosphere vertical region from the surface to about height of 300 km is used in the current work.

The MUAM has radiation module which uses several parameterizations such as varying over days and seasons atmosphere heating and cooling. The first one takes into account the ultraviolet and visible spectral bands (125–700 nm), the second one is the 8, 9.6, 14 and 15 μm infrared bands. Additional dynamic heat sources, parametrization of molecular as well as turbulent viscosity, ion drag, and thermal conductivity are also involved in the lower thermosphere of the model. Planetary waves can be excited at the lower boundary of the model corresponding to the Earth's surface. Tropospheric changes such as cloudiness and weather conditions are not modeled. The MUAM make allowance for three parameterizations of gravity waves (GW). Different phase velocities GW, specifically orographic waves are included.

The model can simulate planetary waves such as stationary planetary waves (SPWs), the eastward waves, defined as Kelvin waves, westward travelling atmospheric normal modes (NMs) (Pogoreltsev et al. 2014). To simulate various PWs the heat balance equation is modified with the additional terms of the form of time-dependent sinusoidal harmonics. The zonal wavenumbers m of these harmonics are 1 and 2; periods are matching to simulated PWs. The method given by Swarztrauber and Kasahara (1985) for Hough functions is used to adjust the latitude structures of NM units. Thuswise, atmosphere reacts to the wave

influence at low boundary and the periods of this reaction are resonant and equal to the NMs periods (Pogoreltsev 1999). When conducting model experiments, (1,1), (1,2), (1,3), (2,1), and (2,2) NMs in the Longuet-Higgins classification (1968) were considered. Under ideal conditions in a non-dissipative atmosphere and in the absence of background wind, these normal modes correspond to waves with periods of 5, 10, 10, 4, 7 days, respectively. But in the real atmosphere, in the presence of external factors, such as the dissipation and inhomogeneous stratification, the spectra of PW are blurred and shifted from the classical behavior (this is clearly shown in figures showing wavelet spectra below). Therefore, when designating such waves, the prefix "quasi" is often used. For example, in the works of Yamazaki & Matthias (2019); Yamazaki et al. (2021) it was shown that the period of PW may vary when measured at different latitudes, and the mean period of 4-day PW is 3.8 ± 0.4 days. For simplicity, we do not use the prefix "quasi". The NMs sources specified in the MUAM give the amplitudes of the modeled waves comparable to those observed in the stratosphere (Pogoreltsev et al. 2009).

2.2 Settings of the model run experiments

In Koval et al. (2023) work, MUAM numerical experiment is described. It implied a series of model runs which were conducted for January–February conditions to evaluate variability of the global circulation as a response of various wave components influence. Ultrafast wave with period of about 3.5 days, zonal number $m=1$ (Kelvin wave) travelling to the east; NMs with periods of about 5, 10, 16 days ($m=1$) and with periods of about 4 and 7 days ($m=2$) travelling to the west were considered. Geopotential height fields were expanded into the four harmonics ($m=1$–4) with the longitude-time Fourier expansion to obtain the PW amplitudes. Then the least squares approximation to the given oscillation periods was carried out.

The conducted model experiments differed by turning on/off the studied PW sources, i.e., model run No.1 (a reference run) was realized to calculate the atmospheric circulation with the integration of all considered PWs sources. The other runs implied the tuning off the individual waves sources (Koval et al. 2023). Comparison of the amplitudes variations in the geopotential height (the run No.1) for each wave with the amplitudes of the same waves according to the results of the model experiment with the wave source switched off showed the omission of waves excitation in the model middle atmosphere, and the PW amplitudes with the sources switched off could be considered as a numerical noise. Such a conclusion was valid with respect to the Kelvin wave and all NMs with the exception of the 16-day PW. It was shown that a 16-day PW in the southern lower thermosphere (about 62.5° S; 110 km altitude) existed independently of the tropospheric source. The largest amplitude variations in geopotential height reach 15 m during the switching off the wave source in the troposphere, whereas it is about 24 m for the turned-on case. Thus, a phenomenon of 16-day PW excitation by intrinsic model atmospheric sources was revealed. The presented below nonlinear PW interaction mechanism, capable of generating secondary PW, was considered to interpret this effect.

2.3 Nonlinear interaction of atmospheric waves

PWs exhibit their spatial inhomogeneity while propagating in nonlinear systems such as the atmosphere. The waves nonlinear influence each other, generate secondary waves and interact with the mean flow. One of the ways to study such influences and interactions, taking into account the generation of secondary PW, is to study the pertubed potential enstrophy, which is the potential vorticity squared. The balance equation of the eddy potential enstrophy is obtained from to the conservation equation of potential vorticity, while various variants of the potential vorticity are possible. For instance, potential vorticity for the case of quasi-geostrophic approximation was used to obtain the quasi-geostrophic eddy potential enstrophy equation in early papers (Smith 1983). Subsequently, for example, in Pogoreltsev and Sukhanova (1993), it was noted that the use of quasi-geostrophic quantities and approximations is not always justified, in particular while modeling stationary PWs. Vanishing of the geopotential (or pressure) disturbances at the equator is the consequence of quasi-geostrophic approximation using, which in turn leads to total isolation of the hemispheres while modeling, since there is no exchange of wave energy between the hemispheres. An Ertel's potential vorticity is used in this work to obtain the eddy potential enstrophy equation. Such a vorticity, unlike quasi-geostrophic potential vorticity, is a dynamic quantity describing both dynamic (vorticity) and thermodynamic (potential temperature) properties (Haynes and McIntyre 1987) and is implied the quasi-geostrophic approximation rejection.

Recently, Didenko et al. (2022) presented a transformation of the pertubed potential enstrophy equation for a detailed specification of the potential enstrophy balance and analysis of nonlinear wave processes. The common form of the eddy potential enstrophy balance can be conceived as:

$$\begin{aligned}\frac{1}{2}\frac{\partial\overline{P'}^2}{\partial t} &= -\overline{P'\left(\vec{V'}\cdot\vec{\nabla}P'\right)} - \frac{1}{\rho o}\mathrm{div}\left(\rho o\overline{P}\overline{P'\vec{V'}}\right)\\ &\quad -\overline{P'\left(\vec{\overline{V}}\cdot\vec{\nabla}P'\right)} + \overline{P}\overline{\left(\vec{V'}\cdot\vec{\nabla}P'\right)} + \overline{P'S'}.\end{aligned} \tag{1}$$

Here P is the Ertel's potential vorticity; $\overrightarrow{V}$–wind vector which includes zonal, meridional and vertical components; S presents terms describing the additional contributions to the momentum equation and diabatic outflows and inflows; ρ_0 is the density being a height-dependent function only. The lines at the top means zonally averaged components and the primes define the deviation from the zonally averaged values or perturbations.

In Smith et al. (1984) and White et al. (2015) works, the Eq. (1) left side terms described as a measure of wave activity time variations or wave transience. The terms responsible for the nonlinear interactions between planetary waves, the divergence and advection of potential enstrophy flux, nonlinear interactions between planetary waves and mean flux, the dissipation are defined the right part of the Eq. (1).

In this context, any perturbation in Eq. (1) with wavelength λ, frequency ω and phase ϕ is approximated by the zonal harmonics sum with m from 1 to infinity. For example, the disturbance of the Ertel's potential vorticity:

$$P\prime = \sum_{m=1}^{\infty} (P_{mc}\cos(m\lambda - \omega t - \varphi) + P_{ms}\sin(m\lambda - \omega t - \varphi)). \quad (2)$$

Since Eq. (1) describes various nonlinear processes, including interactions between PWs, the generation of secondary PW when obtaining the equation of eddy potential enstrophy for individual wave modes are also should be considered. When a signal representing two cosine/sinuous waves with m numbers and ω frequencies ($m1$, $\omega 1$) and ($m2$, $\omega 2$) get through some quadratic system come out to be nonlinear, the signal at the system's output will be a secondary wave ($2m1$, $2\omega 1$), ($2m2$, $2\omega 2$), ($m1-m2$, $\omega 1-\omega 2$) and ($m1+m2$, $\omega 1+\omega 2$). Using the numerical modeling results of NMs, the contribution from both nonlinear interactions between PWs and nonlinear self-interactions were shown by Pogoreltsev (2001). This theory is used in this work with a view to calculate explicitly the eddy potential enstrophy variations of the wave with a 16-day period during January–February, as well as the contribution made to this change by the nonlinear interactions of other PWs.

To test the feasibility of modeling wave structures in MUAM, data from the EOS MLS (The Earth Observing System Microwave Limb Sounder) instrument onboard the Aura satellite (Waters et al. 2006) and The Modern-Era Retrospective analysis for Research and Applications, Version 2 (MERRA-2, Gelaro et al. 2017) were used. To obtain values at regular grid nodes, corresponding to MUAM, the spatially irregularly distributed MLS remote sensing data are interpolated using the natural neighbor method onto a grid with a spatial resolution of $5^\circ \times 5.625^\circ$ (latitude and longitude, respectively) for each pressure level. The geopotential height long-time matrices at fixed latitude are subjected to Fourier transform to obtain time series of individual zonal harmonics amplitudes and phases (Yamazaki 2023). Further, the time series of amplitudes and phases of the westward and eastward propagating planetary waves are obtained using the complex Morlet wavelet transform (Torrence & Compo 1998).

3 Results

3.1 Amplitudes of planetary waves in January and February

An amount of numerical experiments were implemented with the MUAM for various scenarios with selective switching on/off of tropospheric sources of individual PW modes with periods of 4–16 days (see Koval et al. 2023), to explain the observed effect of 16-day PW generation in the lower thermosphere of Southern Hemisphere. Figure 1a shows the amplitudes of the 16-day PW averaged over January (left panels) and February (right panels) according to the MUAM results with all the considered waves' sources included. Grey lines determine the structure of the waveguide. The waveguide of the PW concept characterizing atmospheric regions where the profiles of background wind and temperature contribute to propagation of PW was proposed by Dickinson (1968). Later, Matsuno (1970) introduced the zonal-mean refractivity index squared with respect to the quasi-geostrophic approximation under the assumption that the strongest propagation of a PW occurs in areas with major positive index values, and wave attenuation in its negative values. The regions of the positive refractive index are located equatorward from the specified contours. In general, the distribution of the structure of the 16-day PW is typical for the winter season: the maximum amplitude is achieved in the winter stratosphere, while in the southern stratosphere there is a barrier to wave propagation associated with a strong easterly wind. In this region in Fig. 1a, the region of negative refractive index is prominent. In the mesosphere, the wind turns eastward, a waveguide appears again, and the wave propagates into the lower thermosphere and above in both hemispheres. The simulated distribution of zonal mean zonal wind from the relevant MUAM model run is presented in Fig. 3 of Koval et al. (2023).

The PW structure corresponds to reanalysis data, satellite, radar observations (Pancheva et al. 2008, 2010; Forbes and Zhang 2017; Pedatella and Forbes 2009; Huang et al. 2017) and previous studies of general circulation of the atmosphere and its wave components (e.g., Gavrilov et al. 2018; Koval et al. 2018a). For a more

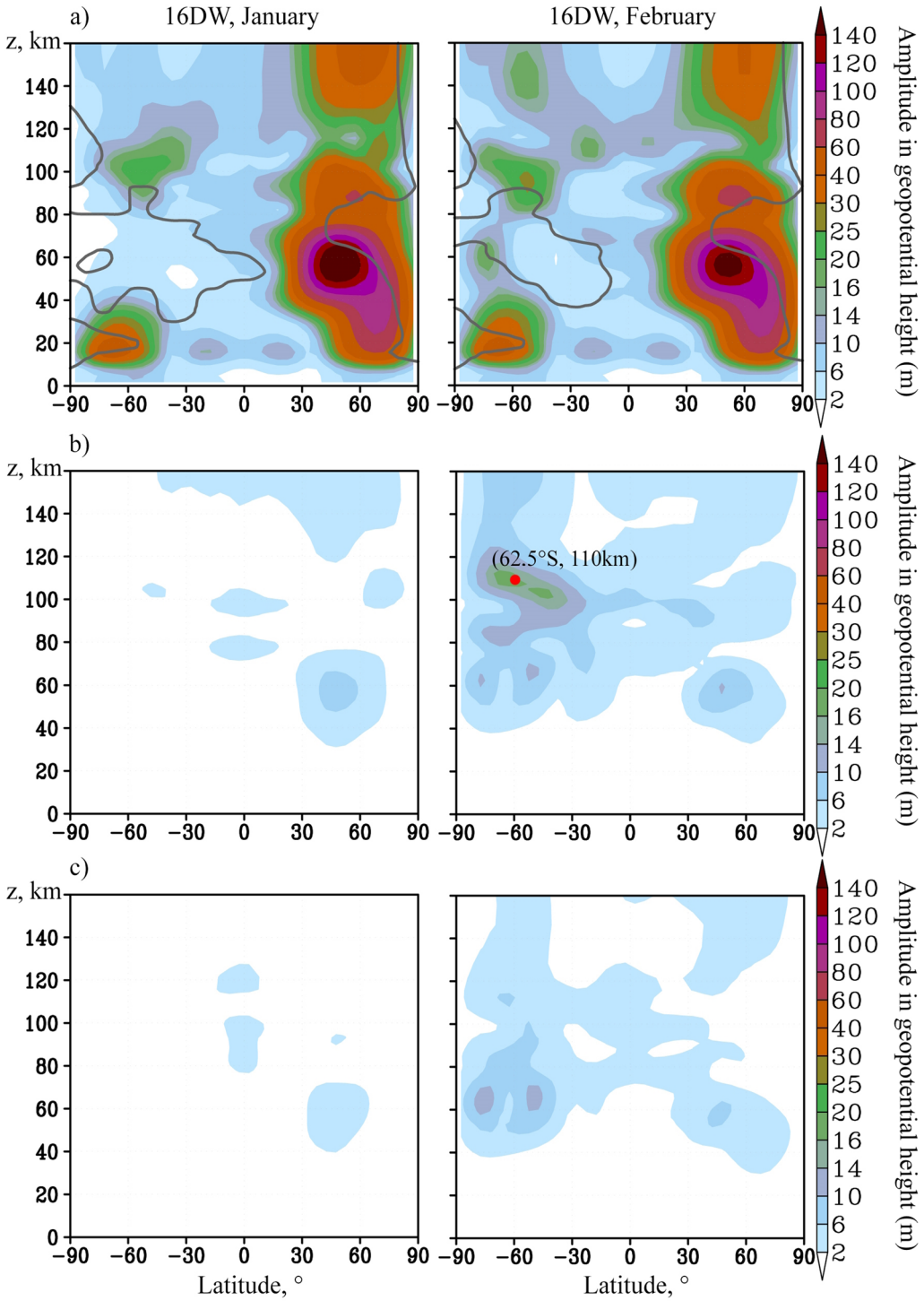

Fig. 1 Amplitudes of the 16-day PW. Geopotential height variations (m) caused by the 16-day PW averaged over January (left panels) and February (right panels): **a** MUAM simulations with included sources of all PWs. Grey contours show borders of waveguides, that are located equatorward from the gray lines; **b** 16-day PW source switched off; **c** 4, 5 and 16 days PWs switched off

detailed analysis of the possibility of PW modeling in the MUAM model, in the "Discussion and summary" section a comparison is also made of the constructed wavelet spectra of PW according to MUAM data, satellite remote sensing and reanalysis. In addition, a comparison was made for 16-day variations in PW amplitudes of various

hydrodynamic fields (except for geopotential height) according to the model data (Koval et al. 2018b), as well as those presented in the work of McDonald et al. 2011; Gong et al. 2019 and Li et al. 2021 show good agreement.

It can be concluded that the MUAM data are consistent with the data from the above studies, and it reliably reproduces the observed PW amplitudes.

Figure 1b shows similar distributions of 16-day PW amplitudes, but for a model scenario with the tropospheric source of this wave turned off. There is an area marked with a red dot where the 16-day wave is observed regardless of the source in the troposphere in February (Fig. 1b–right panel). Thus, it is obvious that in February in the Southern Hemisphere lower thermosphere the westward propagating 16-day PW amplitude decreased by only 10% when the source of the wave was turned off.

Due to the amplitudes maxima of 4 and 5-day waves in the southern lower thermosphere in the MUAM, it was suggested that the essential source of the 16-day wave in this region at the same heights as the area marked with a red dot (see Fig. 2) is the nonlinear interconnection of 4 and 5-day waves.

The generation of a 16-day PW as a result of nonlinear interactions of a 4- and 5-day waves' assumption is explained by the theory of secondary PW occurrence described in the previous section. According to the theory, interacting of two waves results in a secondary wave with the zonal wave number m and frequency which can match with the sum or difference of the parent waves. As was mentioned above, the sources of 4-, 5- and 16-day waves (zonal wave number $m = 2, 1, 1$, respectively), with periods of 90, 120 and 360 h, which conforms to frequencies 3.09, 2.3 and 0.7 (10 − 6 Hz), are the additional terms in the MUAM heat balance equation. Periods and frequencies values are justified by the fact that PW are characterized by a strong quasi-periodicity, i.e., the data

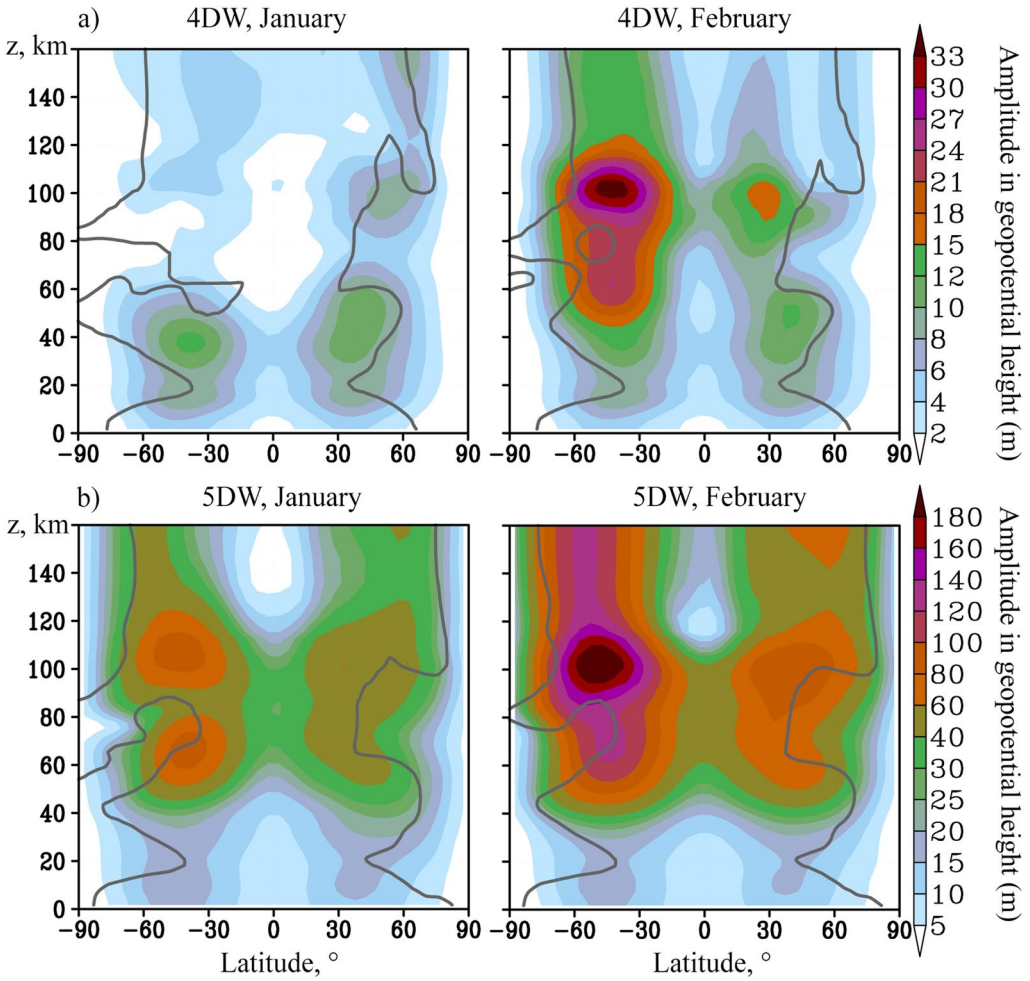

Fig. 2 Amplitudes of the 4 and 5 days PWs. Geopotential height variations (m) caused by the 4 and 5 days PWs (**a**, **b,** respectively) averaged over January (left panels) and February (right panels). Grey contours show borders of respective waveguides (positive refractive indices), that are located equatorward from the gray lines. Note that the color scale is uneven

contain nonstationary power at many different frequencies (Pogoreltsev 2007). Therefore, the wave number and frequency of a 16-day PW is the difference between the wave numbers and frequencies of 4- and 5- day waves. Considering the 16 day wave method generation, the Eq. (1) of eddy potential enstrophy for this PW can be represented as:

$$\begin{aligned}\frac{1}{2}\frac{\partial \overline{P'^{2}_{16}}}{\partial t} = & -\overline{P'_{16}\left(\overrightarrow{V'_4}\cdot\vec{\nabla}P'_5\right)} - \overline{P'_{16}\left(\overrightarrow{V'_5}\cdot\vec{\nabla}P'_4\right)} \\ & -\frac{1}{\rho o}\mathrm{div}\left(\rho o\overline{P}\overline{P'_{16}\overrightarrow{V'_{16}}}\right) - \overline{P'_{16}\left(\overrightarrow{\bar{V}}\cdot\vec{\nabla}P'_{16}\right)} \\ & +\overline{P}\overline{\left(\overrightarrow{V'_{16}}\cdot\vec{\nabla}P'_{16}\right)} + \overline{P'_{16}S'_{16}}\end{aligned} \quad (3)$$

where the subscripts are the wave periods in days. It follows from Eq. (3) that the change in the 16-day PW wave activity (the left part term of the equation) is determined by nonlinear interactions between the waves (the first two terms in the right part), divergence and advection of the potential enstrophy flow (the third and fourth terms in the right part), interaction of the 16-day PW with the mean flow and dissipation (the fifth and sixth terms in the right part).

Figure 2 shows amplitude distributions of 4- and 5-day PWs averaged over January (left) and February (right) calculated for a scenario with the sources of these waves included. We consider wave amplitudes in region (62.5° S; 110 km altitude) marked by red dot in Fig. 1b. Figure 2a shows the increase of wave amplitudes in February relative to January in the region under consideration. The amplitudes of the 5-day wave here rise by 2 times, and the 4-day wave by 8 times.

The structures of westward propagating NMs are subject to strong temporal (as well as interseasonal, see "Discussion and summary") variability. Figure 2a demonstrates, in particular, that in the southern lower thermosphere there is an intensification of the 4- and 5-day wave in February. This may be explained by the variability of the background wind fields. In particular, the speed and direction of the wind in the stratosphere determines the structure of the waveguide along which the wave propagates upward. Figure 2 shows that the waveguide is located closer to the equator and is limited by gray contours. It can be seen that in Fig. 2a in January in the southern stratosphere, the waveguide is interrupted, according to the refractive index formula (Albers et al. 2013), as the easterly jet stream in this area surpasses the phase velocity of the 5-day wave (see also discussion in Koval et al. 2018b). And for the 4-day PW (Fig. 2b) in January, the waveguide region in the stratosphere is narrower than in February.

The MUAM run with the sources of three waves (4-, 5- and 16-day PW) turned off was carried out to verify indirectly the assumption of 16-day wave generation through the nonlinear interaction of 4- and 5-day PW. Figure 1c shows the amplitudes of the 16-day PW based on this model scenario for January and February. Indeed, the amplitudes of the 16-day wave almost disappear both in January and February in the considered lower thermosphere region of the Southern Hemisphere when all three sources are turned off. Thus, the effect of 16-day PW generation, shown in Fig. 1b, by 4- and 5-day waves is confirmed. In the next subsection, we demonstrate the interaction of these primary waves through the balance equation of the perturbed potential enstrophy.

3.2 Eddy potential enstrophy variations of the 16-day PW

The terms in Eq. (3) were calculated using the hydrodynamic quantities fields obtained from the MUAM run with switched off source of the 16-day wave when the wave was observed regardless of its tropospheric source (Fig. 1b). Calculations were carried out for January and February, at 110 km altitude and results were averaged over 52.2°− 67.5° S latitudinal band. Figure 3a shows the calculating results of the potential enstrophy evolution of the 16-day PW, i.e., the left part of Eq. (3) term. The oscillation of the eddy potential enstrophy with of about 16-days period equivalent to the period of the wave under consideration is clearly distinguishable. The sum of the second and third terms of Eq. (3) corresponding to the nonlinear interactions between 4- and 5-day PW provided the generation of the 16-day wave, which is determined as a secondary, is shown in Fig. 3b. The units are $10^{12}(\mathrm{kg{\cdot}m^{-3}})^2{\cdot}\mathrm{PVU}^2/\mathrm{day}$, where 1PVU (potential vorticity unit) $= 10^{-6}\ \mathrm{K{\cdot}m^2{\cdot}kg^{-1}{\cdot}s^{-1}}$.

Figure 3a shows that the change in wave activity defining in the evolution of 16-day wave eddy potential enstrophy starts in early February with a maximum on February 26. Such a behavior of wave activity is in agreement with the previously obtained results presented in Fig. 2 as concerning to 4- and 5-day waves maximum amplitudes in February. Beyond that, the values presented in Fig. 3b are comparable to the values in Fig. 3a. This allows us to conclude that the change in wave activity of the 16-day wave is basically due to nonlinear interactions between the planetary waves under consideration. The generation of secondary PW also begins in early February with maximums observed during the period from February 15 to February 23. The contribution of terms responsible for the interaction of 16-day wave with the mean flux, divergence and advection of the eddy potential enstrophy flow balance and, as a consequence, to the wave activity variations is not significant. The most obvious examples to illustrate are the calculation results of 16-day PW

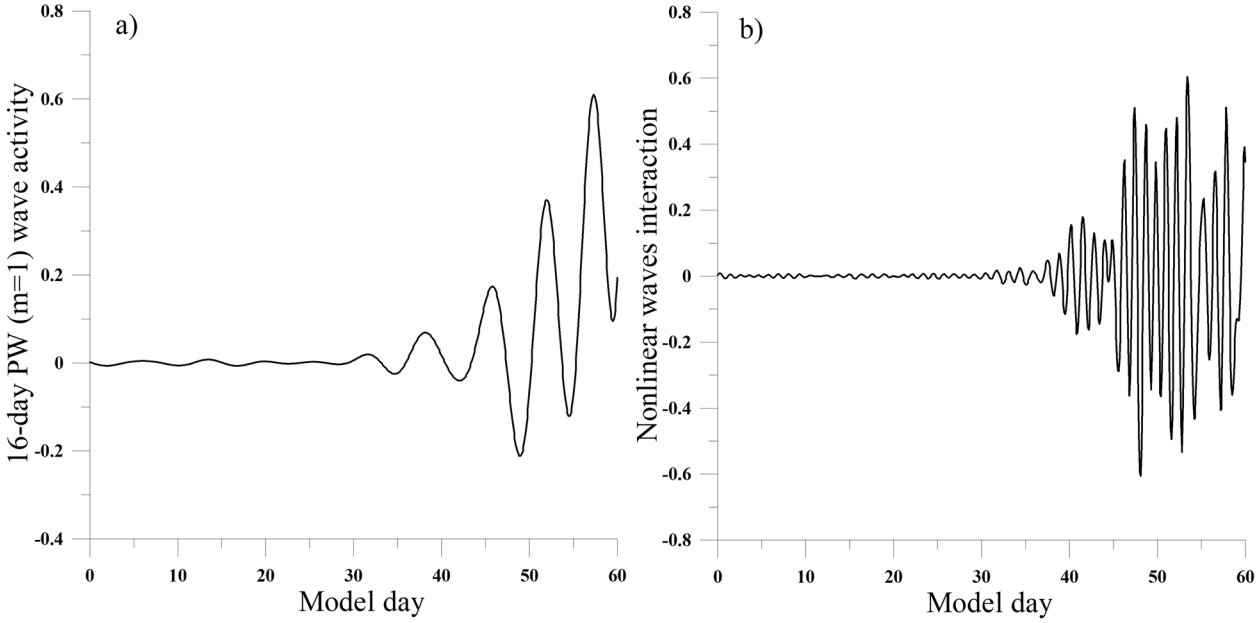

Fig. 3 Terms in balance equation of perturbed potential enstrophy. Evolution of perturbed potential enstrophy of 16-day PW—**a** 4- and 5-day wave-wave interconnections contribution in the balance of the perturbed potential enstrophy—**b** at 52.2°– 67.5° S, 110 km during January–February. Units are 10^{12}(kg m^{-3})^2·PVU^2/day, where 1PVU = 10^{-6} K m^2 kg^{-1}·s.$^{-1}$

interaction with the mean flow in Fig. 4. These results are obtained for the same area as in Fig. 3. The contribution of wave-mean flux interaction is also increasing in February, but the values shown in Fig. 4, less by several orders of magnitude.

The comparison of results in Figs. 3 and 4 demonstrates that both the wave activity variations of the 16-day PW and their maximum values are due to the nonlinear interconnection between PW. Moreover, the mean flow does not affect variations in wave activity.

4 Discussion and summary

In the previous study (Koval et al. 2023), a numerical simulation was carried out implying the initialization of the three-dimensional nonlinear mechanistic numerical model of the global circulation of the middle and upper atmosphere MUAM for January–February dynamic conditions. The obtained hydrodynamic fields and their further numerical processing made it possible to evaluate the relative contribution of various planetary waves' impact to the thermodynamic regime and its variations in the atmospheric layers up to the heights of the thermosphere. The scenarios of the model experiment implied switching on/off the individual PW sources, which are specified in the MUAM. Despite the tropospheric PW sources shaped in the model, the phenomenon of 16-day PW excitation arise out of internal atmospheric sources in the southern lower thermosphere was discovered

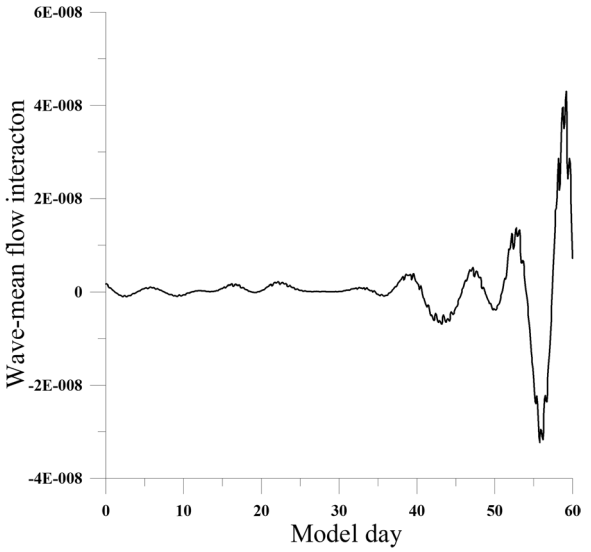

Fig. 4 The term in balance equation of perturbed potential enstrophy. The term responsible for 16-day PW-mean flux interactions in the balance of the eddy potential enstrophy equation at 52.2°– 67.5° S, 110 km during January–February. Units are 10^{12}(kg·m^{-3})^2·PVU^2/day, where 1PVU = 10^{-6} K·m^2·kg^{-1}·s.$^{-1}$

during the experiment. The study of this phenomenon formed the basis of the current study. The results of numerical modeling with switching off the sources of various PW modes showed that the mechanism of

secondary 16-day PW observed in the region of lower thermosphere excitation is 4- and 5- day PWs nonlinear interconnections.

To confirm this fact and to demonstrate explicitly the interaction of the 4- and 5-day waves leading to secondary 16-day PW generation, the equation of the eddy potential enstrophy balance was modified for 16-day PW, taking into account the nonlinear interaction of primary waves. Consideration of this equation terms allowed to demonstrate explicitly the generation of 16-day PW with a zonal wave number $m=1$, in response to the nonlinear interconnection between a 4-day PW with a zonal wave number $m=2$ and a 5-day PW with a zonal wave number $m=1$. The calculation results showed that the terms related to nonlinear PW generation in the eddy potential enstrophy equation are dominant in the 16-day PW activity variations. Moreover, the maximum changes are detected in February, when the 4- and 5-day wave's amplitudes also reach their maximum values in the observed region.

A natural question arises: what is the realism of the meteorological fields reproduced by MUAM in general and PWs in particular. This question has already been discussed many times in previous studies: when comparing modeling data with observational data (e.g., Medvedeva et al. 2019; Koval et al. 2018b; 2022). It was shown that the MUAM satisfactorily reproduces the wind, temperature and spatiotemporal structure of PWs. In this study, we decided to expand the comparison and constructed wavelet spectra of PWs propagating westward according to MUAM simulation, also according to MLS and MERRA-2 data. Figure 5 shows examples of such spectra, calculated in the region of maximum amplitudes of the 16-day PW (as shown in Fig. 1a, this is 62.5° N and 60 km altitude). Left panels show spectra according to MERRA-2 data for different years (Fig. 5a, b, c: 1990, 2013 and 2018). Right panels show similar distributions for different MUAM runs. Figure 5d corresponds to the MUAM run used in this study (when all PW sources are included). Figure 5e and f represents the MUAM runs used in studying the influence of the QBO on the atmospheric circulation (Koval et al. 2022). The sources of waves in the model are the same, the difference between the simulations is only in the presence of a procedure for nudging the zonal wind to the easterly (Fig. 5e) and

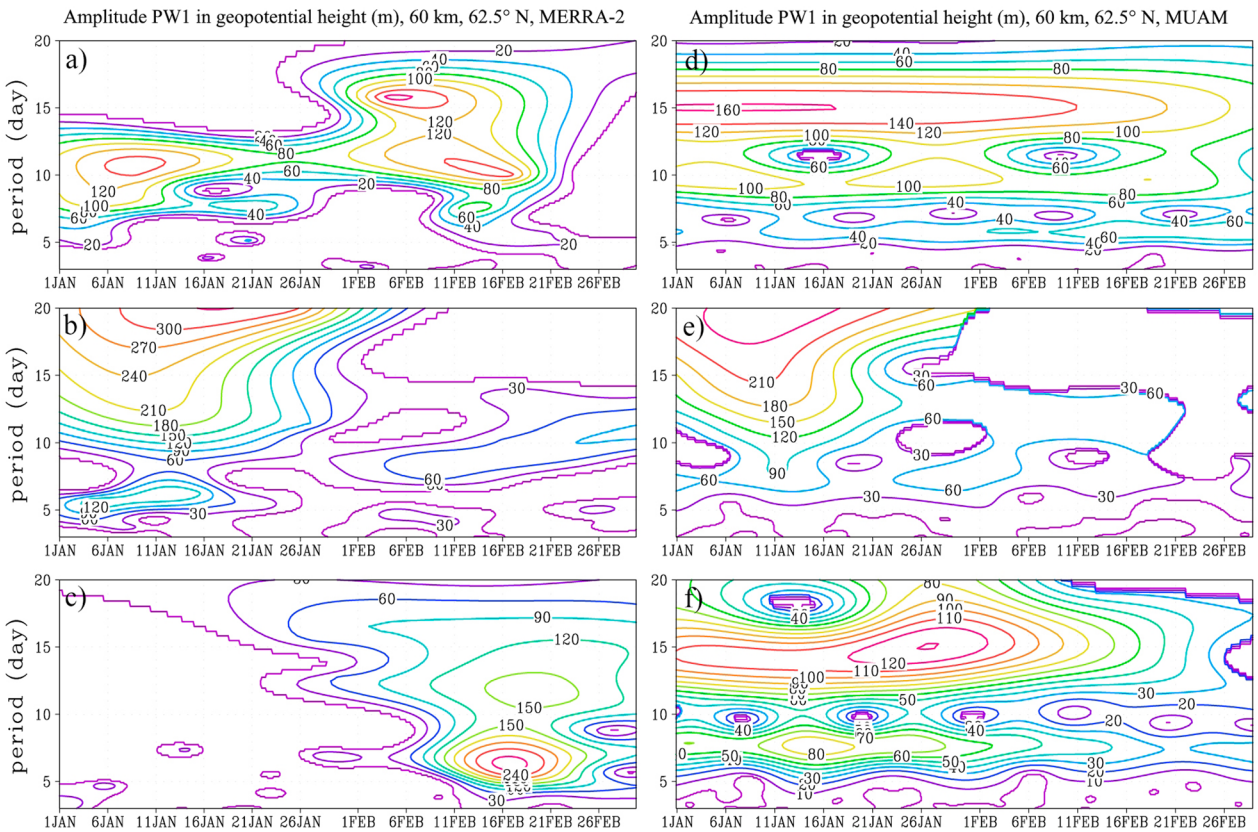

Fig. 5 Time series of amplitude wavelet spectra. Westward propagating PWs with zonal wave number 1 in geopotential height at 60 km, 62.5° N: **a**, **b**, **c**—according to MERRA-2 data; **d**, **e**, **f**—according to MUAM simulations (see text for details)

westerly (Fig. 5f) QBO phases, which is described in the corresponding article.

From Figs. 5a, b, c, a strong variability of PW amplitudes is visible, both temporal and interannual one, observed according to MERRA-2 data. We performed similar calculations of wavelet spectra using MLS data (see the "Methods and approaches" section). Figures with MLS data are not presented here, because they are generally similar to the MERRA-2 for the corresponding time intervals. Figure 5d, e, f demonstrates that MUAM reproduces interannual variability: here it is interpreted as the difference between runs (ensembles of simulations are built on this principle when analyzing climate data, e.g., Pogoreltsev et al. 2007). The amplitude values of the simulated PWs also correspond to reanalysis and satellite remote sensing data.

In addition, we compared the spectra of geopotential height variations in the region of southern lower thermosphere, in which the process of generating a 16-day wave was considered (marked with a red dot in Fig. 1b). For comparison, only MLS data at 100 km altitude were used here. Spectra constructed for different years also show significant interannual variability. Figure 6a, b shows examples of wavelet spectra in the winter of 2020–2021, for PWs with zonal numbers 1 and 2, respectively. Figure 6c, d represents similar distributions according to the model—for the run studied in this article. Although the amplitude values in the Fig. 6 are very different, the similarity of the general structure of oscillations is important here: in Fig. 6a, c (wave number 1) we see in February maximums at periods close to the 5- and 16-days, and in Fig. 6b, d (wave number 2) we see the maximum close to the 4-day wave. This, on one hand, demonstrates the feasibility of coexistence in the real atmosphere of NMs with the periods under consideration. This may indirectly indicate the generation of a 16-day wave by the mechanism considered in this study. On the other hand, this demonstrates the realism of the oscillations modeled in MUAM.

PW propagation and secondary PW generation, as a result of nonlinear interactions, play an essential role in the formation of the Earth's and other planets dynamic regime, as well as in the intercoupling of atmospheric layers, including the atmosphere–ionosphere coupling. As was shown in present study, wave interactions can significantly influence the development of wave motions, therefore, further investigations in the direction of nonlinear PW effects should throw a great deal of light on the solution of the above-mentioned problems. In addition to the generation of a secondary 16-day wave, which is the difference in frequencies and wave numbers of 4- and 5-day waves, the model also generates a secondary 2-day wave (the sum of frequencies and wave numbers of these waves) despite the absence of a separate 2-day wave source in the MUAM. At the same time, its spatial structure coincides with the structure of 4- and 5-day waves, and an increase in its amplitude in February is also noticeable, coinciding with the strengthening of primary waves. However, due to the fact that 2-day wave is not always secondary and

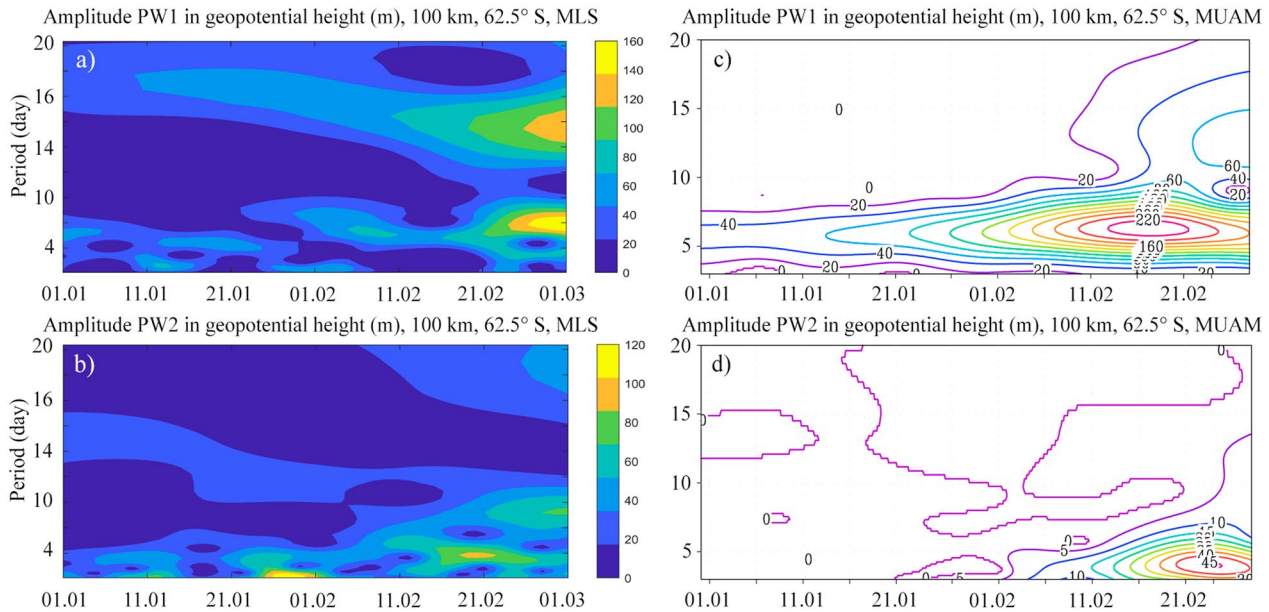

Fig. 6 Time series of amplitude wavelet spectra. Westward propagating PWs in geopotential height: **a**, **b**—based on MLS data at 100 km, 62.5° S: **c**, **d**—based on MUAM simulation at 110 km, 62.5° S. Upper plots show PWs with zonal number 1, bottom plots show zonal number 2

tends to intensify in February, a more detailed study of this wave is a subject for future research.

Abbreviations

MUAM	Middle and upper atmosphere model
PW	Planetary wave
SSW	Sudden stratospheric warming
QBO	Quasi-biennial oscillation
ENSO	El Nino Southern Oscillation
NM	Normal mode
GW	Gravity wave
SPW	Stationary planetary wave
PVU	Potential vorticity unit

Author contributions

All authors made relevant contributions in writing and drafting of the manuscript, data analysis and imaging of the results. K.A.D.: conceptualization, nonlinear wave processes and wave activity variations evaluation, writing the final manuscript; A.V.K.: conceptualization, numerical modeling, consulting and proofreading; T.S.E.: consulting, English editing; O.N.T.: data processing, numerical simulations; A.V.S.: MLS data processing.

Funding

The research was supported by Russian Science Foundation: grant #20–77-10006-P, https://rscf.ru/en/project/20-77-10006/ – MUAM configuration, implementation of numerical modeling of the atmospheric global circulation; grant #23–77-01035, https://rscf.ru/en/project/23-77-01035/ – calculation of PW structures and nonlinear wave processes, analysis of wave activity variations.

Availability of data and materials

In accordance with the statement 1296 of the Civil Code of the Russian Federation, Russian State Hydrometeorological University (RSHU) has all rights on the MUAM code. A permission for computer code usage access is needed for a reader from the RSHU Rector at the address 79, Voronezhskaya street, St. Petersburg, Russia, 192007, phone: 007 (812) 372-50-92. It is possible to obtain such permission with the assistance of the authors. All presented patterns in the paper are archiving to Zenodo. Graphical information in this study is obtained using Grid Analysis and Display System (GrADS) that is a free software developed by to the NASA Advanced Information Systems Research Program and Grapher which is a software program developed by Golden Software.

Declarations

Ethics approval and consent to participate

Not applicable.

Consent for publication

Not applicable.

Competing interests

The authors declare no competing interests.

Author details

[1]Pushkov Institute of Terrestrial Magnetism, Ionosphere, and Radio Wave Propagation (IZMIRAN), Russian Academy of Sciences, Troitsk, Moscow, Russia. [2]Saint Petersburg State University, Saint-Petersburg, Russia. [3]Russian State Hydrometeorological University, Saint-Petersburg, Russia.

Received: 26 April 2024 Accepted: 19 September 2024
Published online: 29 September 2024

References

Albers JR, McCormack JP, Nathan TR (2013) Stratospheric ozone and the morphology of the Northern Hemisphere planetary waveguide. J Geophys Res Atmos 118:563–576. https://doi.org/10.1029/2012JD017937

Baldwin M, Ayarzaguena B, Birner T, Butchart N, Butler A, Charlton-Perez A, Domeisen D, Garfinkel C, Garny H, Gerber E, Hegglin M, Langematz U, Pedatella N (2021) Sudden stratospheric warmings. Rev Geophys 59(1):1–37. https://doi.org/10.1029/2020RG000708

Dickinson RE (1968) Planetary Rossby waves propagating vertically through weak westerly wave guides. J Atmos Sci 25:984–1002

Didenko KA, Koval AV, Ermakova TS, Lifar VD (2022) Interactions of stationary planetary waves during winter 2008–2009 and 2018–2019 sudden stratospheric warmings. Proceeding of SPIE 28th international symposium on atmospheric and ocean optics, atmospheric physics. SPIE, Washington

Ermakova TS, Statnaya IA, Fedulina IN, Suvorova EV, Pogoreltsev AI (2017) Three-dimensional semi-empirical climate model of water vapor distribution and its implementation to the radiation module of the middle and upper atmosphere model. Russ Meteorol Hydrol 42:594–600. https://doi.org/10.3103/S1068373917090060

Ermakova TS, Aniskina OG, Statnaya IA, Motsakov MA, Pogoreltsev AI (2019) Simulation of the ENSO influence on the extra-tropical middle atmosphere. Earth Planet Space. https://doi.org/10.1186/s40623-019-0987-9

Forbes JM, Zhang X (2017) The quasi-6 day wave and its interactions with solar tides. J Geophys Res Space Phys 122:4764–4776. https://doi.org/10.1002/2017JA023954

Forbes JM, Zhang X, Maute A (2020) Planetary wave (PW) generation in the thermosphere driven by the PW-modulated tidal spectrum. J Geophys Res Space Phys. https://doi.org/10.1029/2019JA027704

Fröhlich K, Pogoreltsev AI, Jacobi Ch (2003) The 48-layer COMMA-LIM model. Rep Inst Meteorol Univ Leipz 30:157–185

Gavrilov NM, Koval AV, Pogoreltsev AI, Savenkova EN (2018) Simulating planetary wave propagation to the upper atmosphere during stratospheric warming events at different mountain wave scenarios. Adv Space Res 61(7):1819–1836. https://doi.org/10.1016/j.asr.2017.08.022

Gelaro R, McCarty W, Suárez MJ, Todling R, Molod A, Takacs L et al (2017) The modern-era retrospective analysis for research and applications, version 2 (MERRA-2). J Clim 30:5419–5454. https://doi.org/10.1175/JCLI-D-16-0758.1

Gong Y, Wang H, Ma Z, Zhang S, Zhou Q, Huang C, Huang K (2019) A statistical analysis of the propagating quasi 16 day waves at high latitudes and their response to sudden stratospheric warmings from 2005 to 2018. J Geophys Res Atmos 124(12):617–630. https://doi.org/10.1029/2019JD031482

Haynes PH, McIntyre ME (1987) On the evolution of vorticity and potential vorticity in the presence of diabatic heating and frictional or other forces. J Atmos Sci 44(5):828–841

Haynes PH, McIntyre ME, Shepherd TG, Marks CJ, Shine KP (1991) On the "downward control" of extratropical diabatic circulations by eddy-induced mean zonal forces. J Atmos Sci 48(4):651–678

He M, Forbes JM (2022) Rossby wave second harmonic generation observed in the middle atmosphere. Nat Commun. https://doi.org/10.1038/s41467-022-35142-3

He M, Chau JL, Forbes JM, Thorsen D, Li G, Siddiqui TA, Yamazaki Y, Hocking WK (2020) Quasi-10 day wave and semidiurnal tide nonlinear interactions during the southern hemispheric SSW 2019 observed in the northern hemispheric mesosphere. Geophys Res Lett. https://doi.org/10.1029/2020GL091453

Holton JR, Haynes PH, McIntyre ME, Douglas AR, Rood RB, Pfister L (1995) Stratosphere-troposphere exchange. Rev Geophys 33:403–439

Huang Y, Zhang S, Li C, Li H, Huang K, Huang C (2017) Annual and interannual variations in global 6.5 DWS from 20 to 110 km during 2002–2016 observed by TIMED/SABER. J Geophys Res Space Phys. https://doi.org/10.1002/2017JA023886

Jacobi Ch, Schminder R, Kiirschner D (1998) Non-linear interaction of the quasi 2 day wave and long-term oscillations in the summer midlatitude mesopause region as seen from LF DI wind measurements over central Europe (Collm, 52°N, 15°E). J Atmos Sol Terr Phys 60:1175–1191

Koval AV, Gavrilov NM, Pogoreltsev AI, Savenkova EN (2018a) Comparisons of planetary wave propagation to the upper atmosphere during stratospheric warming events at different QBO phases. J Atmos Sol Terr Phys 171:201–209. https://doi.org/10.1016/j.jastp.2017.04.013

Koval AV, Gavrilov NM, Pogoreltsev AI, Shevchuk NO (2018b) Influence of solar activity on penetration of traveling planetary-scale waves from the troposphere into the thermosphere. J Geophys Res Space Phys 123(8):6888–6903. https://doi.org/10.1029/2018JA025680

Koval AV, Gavrilov NM, Pogoreltsev AI, Kandieva KK (2022) Dynamical impacts of stratospheric QBO on the global circulation up to the lower thermosphere. J Geophys Res Atmos. https://doi.org/10.1029/2021JD036095
Koval AV, Toptunova ON, Motsakov MA, Didenko KA, Ermakova TS, Gavrilov NM, Rozanov EV (2023) Numerical modeling of relative contribution of planetary waves to the atmospheric circulation. Atmos Chem Phys 23:4105–4114. https://doi.org/10.5194/acp-23-4105-2023
Labitzke K, Kunze M (2009) On the remarkable Arctic winter in 2008/2009. J Geophys Res. https://doi.org/10.1029/2009JD012273
Li W, Huang C, Zhang S (2021) Global characteristics of the westward-propagating quasi-16 day wave with zonal wavenumber 1 and the connection with the 2012/2013 SSW revealed by ERA-interim. Earth Planet Space 73:113. https://doi.org/10.1186/s40623-021-01431-2
Longuet-Higgins MS (1968) The eigenfunctions of Laplace's tidal equation over a sphere. Philos T R Soc Lond 262:511–607
Matsuno T (1966) Numerical integration of the primitive equations by a simulated backward difference method. J Meteorol Soc Japan 44:76–84
Matsuno T (1970) Vertical propagation of stationary planetary waves in the winter Northern Hemisphere. J Atmos Sci 27(6):871–883
McDonald AJ, Hibbins RE, Jarvis MJ (2011) Properties of the quasi 16 day wave derived from EOS MLS observations. J Geophys Res 116:D06112. https://doi.org/10.1029/2010JD014719
Medvedeva IV, Semenov AI, Pogoreltsev AI, Tatarnikov AV (2019) Influence of sudden stratospheric warming on the mesosphere/lower thermosphere from the hydroxyl emission observations and numerical simulations. J Atmos Sol Terr Phys 187:22–32. https://doi.org/10.1016/j.jastp.2019.02.005
Nath D, Chen W, Zelin C, Pogoreltsev AI, Wei K (2016) Dynamics of 2013 sudden stratospheric warming event and its impact on cold weather over Eurasia: role of planetary wave reflection. Sci Rep. https://doi.org/10.1038/srep24174
Pancheva D (2000) Evidence for nonlinear coupling of planetary waves and tides in the lower thermosphere over Bulgaria. J Atmos Sol Terr Phys 62:115–132
Pancheva D, Mukhtarov P, Mitchell NJ, Merzlyakov E, Smith AK, Andonov B, Singer W, Hocking W, Meek C, Manson A, Murayama Y (2008) Planetary waves in coupling the stratosphere and mesosphere during the major stratospheric warming in 2003/2004. J Geophys Res. https://doi.org/10.1029/2007JD009011
Pancheva D, Mukhtarov P, Andonov B, Forbes JM (2010) Global distribution and climatological features of the 5–6 day planetary waves seen in the SABER/TIMED temperatures (2002–2007). J Atmos Sol Terr Phys 72(1):26–37. https://doi.org/10.1016/j.jastp.2009.10.005
Pedatella NM, Forbes JM (2009) Modulation of the equatorial F-region by the quasi-16 day planetary wave. Geophys Res Lett. https://doi.org/10.1029/2009GL037809
Pogoreltsev AI (1999) Simulation of planetary waves and their influence on the zonally averaged circulation in the middle atmosphere. Earth Planet Space 51(7/8):773–784
Pogoreltsev AI (2001) Numerical simulation of secondary planetary waves arising from the nonlinear interaction of the normal atmospheric modes. Phys Chem Earth Part C 26(6):395–403
Pogoreltsev AI (2007) Generation of normal atmospheric modes by stratospheric vacillations. Izv Atmos Ocean Phys 43(4):423–435
Pogoreltsev AI, Sukhanova SA (1993) Simulation of the global structure of stationary planetary waves in the mesosphere and lower thermosphere. J Atmos Sol Terr Phys 55:33–40
Pogoreltsev AI, Vlasov AA, Froehlich K, Jacobi Ch (2007) Planetary waves in coupling the lower and upper atmosphere. J Atmos Sol Terr Phys 69:2083–2101. https://doi.org/10.1016/j.jastp.2007.05.014
Pogoreltsev AI, Kanukhina AYu, Suvorova EV, Savenkova EN (2009) Variability of planetary waves as a signature of possible climatic changes. J Atmos Sol Terr Phys 71:1529–1539. https://doi.org/10.1016/j.jastp.2009.05.011
Pogoreltsev AI, Savenkova EN, Pertsev NN (2014) Sudden stratospheric warmings: the role of normal atmospheric modes. Geomag Aeron 54(2):1–15. https://doi.org/10.1134/S0016793214020169
Pogoreltsev AI, Savenkova EN, Aniskina OG, Ermakova TS, Chen W, Wei K (2015) Interannual and intraseasonal variability of stratospheric dynamics and stratosphere-troposphere coupling during northern winter. J Atmos Sol Terr Phys 136:187–200. https://doi.org/10.1016/j.jastp.2015.08.008
Smith AK (1983) Observation of wave-wave interactions in the stratosphere. J Atmos Sci 40:2484–2493
Smith AK, Gille JC, Lyjak LV (1984) Wave-wave interactions in the stratosphere: observations during quiet and active wintertime periods. J Atmos Sci 41:363–373
Strang G (1968) On the construction and comparison of difference schemes. SIAM J Numer Anal 5:516–517
Swarztrauber PN, Kasahara A (1985) The vector harmonic analysis of Laplace,s tidal equations. SIAM J Sci Comput 6:464–491
Teitelbaum H, Vial E (1991) On tidal variability induced by nonlinear interaction with planetary waves. J Geophys Res 96(14):179–182
Torrence Ch, Compo GP (1998) A practical guide to wavelet analysis. Bull Amer Met Soc 79(1):61–78
Waters JW, Froidevaux L, Harwood RS, Jarnot RF, Pickett HM, Read WG, Siegel PH, Cofield RE, Filipiak MJ, Flower DA et al (2006) The earth observing system microwave limb sounder (EOS MLS) on the Aura satellite. IEEE Trans Geosci Remote Sens 44(5):1075–1092
White IP, Hua L, Mitchell NJ, Phillips T (2015) Dynamical response to the QBO in the northern winter stratosphere: signatures in wave forcing and eddy fluxes of potential vorticity. J Atmos Sci 72:4487–4507. https://doi.org/10.1175/JAS-D-14-0358.1
Yamazaki Y (2023) 2023) A method to derive Fourier–wavelet spectra for the characterization of global-scale waves in the mesosphere and lower thermosphere and its MATLAB and Python software (fourierwavelet v1.1). Geosc Model Dev 16:4749–4766
Yamazaki Y, Matthias V (2019) Large-amplitude quasi-10 day waves in the middle atmosphere during final warmings. J Geophys Res Atmos 124:9874–9892. https://doi.org/10.1029/2019JD030634
Yamazaki Y, Matthias V, Miyoshi Y (2021) Quasi-4 day wave atmospheric manifestation of the first symmetric Rossby normal mode of zonal wavenumber 2. J Geophys Res Atmos 126:e2021JD034855. https://doi.org/10.1029/2021JD034855

Publisher's Note